https://dx.doi.org/10.4314/dujopas.v11i1c.8
ISSN (Print): 2476-8316
ISSN (Online): 2635-3490
Dutse Journal of Pure and Applied Sciences (DUJOPAS), *Vol. 11 No. 1c March 2025*

Magnetic and Structural Characteristics of Monolayer Chromium Iodide: A Theoretical Investigation

Musa Muhammad Elbulatory[1], Tasiu Zangina[1], Terhemba Shadrach Bem[1], Ibrahim Buba Garba[2] Tahir Abdullahi[3], Abubakar Saidu Shuaibu[1], Chifu E. Ndikilar[1]

[1]Department of Physics,
Faculty of Physical Science,
Federal University Dutse,
Jigawa State,
P.M.B 7156,
Nigeria.

[2]Department of Physics,
Faculty of Science,
Federal University Gashua,
Yobe State
P.M.B 671106,
Nigeria.

[3]Department of Physics,
Faculty of Science,
Yobe State University Damaturu,
Yobe State
P.M.B 1144,
Nigeria.

Abstract

The recent discovery of 2D magnetic systems has inspired research into their fundamental properties and prospective applications. Emerging 2D materials, chromium trihalides (CrX_3, X = Cl, Br, I), exhibit controllable spin-lattice interactions, making them promising material for next-generation technologies in magnonics, spintronic, and magneto electronics. For the investigation of heat transport in a changing magnetic field, CrI_3 stands out as a possible material due to its low-temperature antiferromagnetic (AFM) interlayer interactions. This study employs density functional theory (DFT) to examine the convergence criteria, magnetic characteristics across various magnetic phases, and structural properties of monolayer CrI_3. The results of our convergence tests indicate that the optimized lattice constant is 6.880 Å, which is achieved with an energy cut-off of 40 Ry and a k-point mesh of 7x7x1, corresponding to the minimum total energy. Furthermore, our calculations yield a magnetic moment of 3.56 μB per Cr atom, providing insight into the material's magnetic properties. The optimized lattice constant and magnetic moment obtained in this study provide a fundamental understanding of monolayer CrI_3 properties, paving the way for the development of novel magnetic and electronic devices. These findings have far-reaching implications for the advancement of spintronic, magnonics, and related fields.

Keywords: 2D materials, Chromium Iodide, Ab initio DFT calculations, Total energy, Magnetic moment.

**Author for Correspondence*

INTRODUCTION

Recent years have seen remarkable progress in material science, fueled by the demand for innovative materials with outstanding thermal, electronic, and optical properties. The global demand for solar energy as an abundant resource necessitates more efficient photovoltaic materials to tap into its full potential.

Graphene and other 2D materials can exhibit tunable electronic and magnetic properties when decorated with transition metals (Song et al., 2018). However, the absence of intrinsic magnetism in these 2D materials limits their exploitation spintronic applications because their long-range order cannot withstand fluctuations in temperature in an isotropic system (Mermin-Wagner theorem) (Halperin, 2019). Recent research has shown that the Mermin-Wagner constraint cannot be applied to magnetization of materials at non-zero temperatures in some 2D materials with a significant magneto crystalline anisotropy, such as Chromium (III) Iodide (CrI_3) (Kaur & Mandal, 2024).

Among these materials, CrI_3 stands out due to its intriguing magnetic order and electronic band structure, making it a focal point for spintronic and nanoelectronics applications. This van der Waals material (CrI_3) is easily exfoliated into mono-, bi-, and few-layer structures, granting it exceptional properties (Li et al., 2019) (Gibertini et al., 2019) (Huang et al., 2020). Its layered configuration gives CrI_3 exceptional characteristics, making it an enticing candidate for various technological applications. This potential is further enhanced by the unique interplay between its properties, as phononic, electronic, and magnetic degrees of freedom are strongly coupled, as proved by both theory and experiment (Singh et al., 2019). A study of magneto-phononic phenomena in CrI_3 is desirable because of the material's several degrees of freedom and the potential to use them in nanoscale electro-optical, spintronic, and caloritronic applications as shown in **Fig 1.**

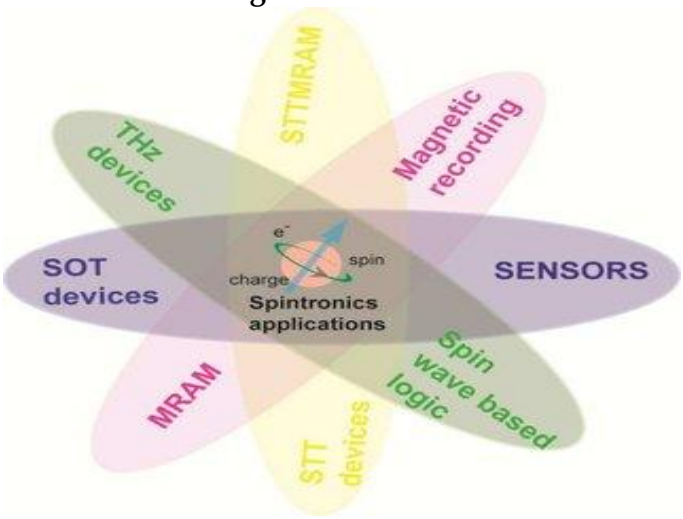

Fig 1: Present and future applications of spintronic (Irfan, 2021).

Permanent magnetic order in atomically thin CrI_3 was experimentally confirmed in 2017, marking the first demonstration of 2D magnetism. Using the polar magneto-optical Kerr effect (MOKE), Experiments and theory agreed that, 2D CrI_3 is a ferromagnetic semiconductor with antiferromagnetic interaction between its layers (Huang et al., 2017). Increases in the number of layers and heterostructures with graphene do not disrupt the magnetic order. Despite its low Curie temperatures (61 K for bulk and 45 K for monolayer), it maintains its ferromagnetic properties far into the high-temperature range, with the monoclinic to rhombohedral phase transition occurring at around 220 K (Tomarchio et al., 2023).

A potent combination of first principles of DFT and Diffusion Monte Carlo (DMC) calculations produced some of the most accurate estimates of the electronic, magnetic, and structural properties of monolayer CrI_3. Based upon the DMC-quality structure obtained and acquired a high-resolution monolayer spin density that showed each Cr atom to possess a magnetic moment of 3.62 μB and each I atom to have a moment of -0.145 μB. As demonstrated, CrI_3 possesses remarkably strong spin-phonon coupling, with a predicted value as large as 3.32 cm-1 (Staros et al., 2022). Mogulkoc et al., (2023) reported that the ground-state electronic structure calculations were performed by using *ab initio* methods based on density functional theory (DFT) and the projected augmented wave (PAW) method as implemented in the Vienna *ab initio* simulation package. Cr*X* systems are dynamically stable and demonstrate ferromagnetism along with half metallicity. 2D phases of chromium pnictides are predicted to be the perfect spin polarizers with ferromagnetic order and room temperature stability. The electronic structure and magnetic properties of monolayer CrI_3 can be the changed by adsorption of alkali metals., calculations show that a lower adsorption coverage of alkali metal can transform monolayer CrI_3 from semiconductor to half metal. The total magnetic moment and the local spin magnetic moment of Cr are linearly enhanced with increasing adsorption coverage, which greatly enhances the ferromagnetism. The method was carried out by DFT implemented on VASP (Yang et al., 2021).

Previous studies on monolayer CrI_3 have employed various pseudopotential methods to investigate its ground-state properties, magnetic and electronic behavior, and vibrational characteristics. However, this work focuses on establishing the convergence criteria and exploring the magnetic and structural properties of the monolayer CrI_3 using the Perdew-Burke-Ernzerh of non-linear core correction Kresse-Joubert Projector-Augmented Wave (PBE-spn-kjpaw) pseudopotential prescription. Notably, this study is the first to report on monolayer CrI_3 using this specific pseudopotential approach. This study lays the groundwork for investigating the vibrational properties of monolayer CrI_3, including phonon dispersion and density of states, which can reveal energy propagation mechanisms within the lattice (Pocs et al., 2020) (Study et al., 2022).

COMPUTATIONAL METHOD

All calculations are performed using the Quantum ESPRESSO (QE) distribution (Giannozzi et al., 2009). We use the exchange-correlation functional constructed using spin-polarized Generalized-Gradient Approximation (GGA) with the Perdew-Burke-Ernzerhof non-linear core correction Kresse-Joubert Projector-Augmented Wave (PBE-spn-kjpaw) prescription within the quantum expresso pseudopotential library (Blöchl, 1994) (Reyes-Martinez et al., 2020). A systematic convergence test was carried out to investigate the convergence behavior of Total Energy (Etot) with respect to Energy Cutoff (Ecut), Lattice Constant (Lat), and Brillouin Zone Sampling (K Points). The ratio of 1:10 for E_{cut} and energy cutoff threshold was used (Wang et al., 2021) (Mañes, 2012). To determine the total minimum energy of CrI_3, we performed calculations using a 7×7×1 k-point mesh (2 Cr and 6 I atoms), taking into account the crystal symmetry, which results in degenerate energy states for certain k-points. The energy cutoff was varied from 10 Ry to 100 Ry (Webster & Yan, 2018) (Tomar et al., n.d.), with the results presented in Table 1. Convergence tests were also conducted with respect to k-point sampling, using mesh sizes ranging from 1×1×1 to 10×10×1 with an interval of 1.0, while keeping the lattice constant and energy cutoff fixed (Tomar et al., n.d.). The results are summarized in Table 2. Furthermore, we calculated the optimal lattice constant for CrI_3 using a hexagonal crystal structure. The calculations employed a plane wave kinetic energy cutoff of 40 Ry and a Monkhorst-Pack grid of 7×7×1 (Olsen, 2019). The results are presented in Table 3. The ferromagnetic moment was computed from Self-consistent Field Calculation (scf)

output file and the structural properties were visualized and computed using VESTA (Retegan et al., 2023) (Aslam et al., 2023) (Wang & Sanyal, 2021).

RESULTS AND DISCUSSION

Convergence Test

The first result presents the total energy of the CrI_3 compound, investigated with respect to three key parameters: energy cutoffs, K-point sampling, and lattice constant (Hamann, 2013).

Total Minimum Energy of CrI_3 with Respect to Energy Cutoffs, k-point and lattice parameters

The convergence of the total energy of CrI_3 with respect to the plane wave cutoff energy was investigated. An increment of energy cutoff for wave function is made until the convergence is achieved. The total minimum energy converged at 40 Ry plane wave cut offs energy and the total ground state energy had its minimum at -2769.88314685 Ry. The total minimum energy increases monotonically with the energy cutoff for the wave function, as shown in Fig. 2. The accuracy of the ground state energy depends on the number of basis functions (Chen et al., 2020). Moreover, when the number of basis functions approaches infinity, the total minimum energy is close to the ground state energy (Daga et al., 2020).

Table 1: Total minimum energy of CrI_3 with respect to energy cutoffs

Energy Cutoff (Ry)	Total Energy (Ry)
10	-2718.98329510
20	-2761.49795862
30	-2769.18773767
40	-2769.88314685
50	-2769.92164406
60	-2769.92578087
70	-2769.93145616
80	-2769.93393961
90	-2769.93461234
100	-2769.93489856

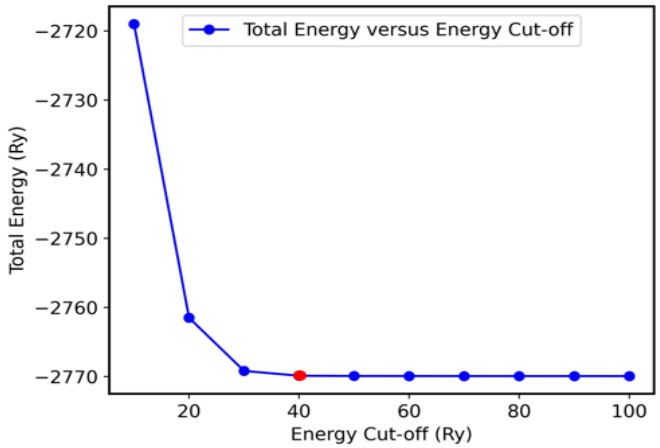

Figure 2: Graph of total minimum energy of CrI_3 with respect to energy cutoffs where 40 Ry (red dot) is shown be the best converged value.

Another convergence test of total energy for K-point sampling was performed on CrI_3. The total energy of CrI_3 was calculated using various sets of K-points ranging from 1× 1 × 1 to 10

× 10 × 1. In each of these cases the plane wave kinetic energy cutoff of 40 Ry was used. The total minimum energy of CrI_3 is calculated as a function of K-points grid size using plane wave self-consistent field code (Novoselov Artem; Carvalho, Alexandra; Neto, A. H. Castro, 2016). For this calculation, the other variables (lattice constant and energy cutoff) are kept constant. Convergence of the total energy with respect to the discrete Brillouin zone sampling was achieved for 7 × 7× 1 Monkhorst-Pack grid (Wang et al., 2021). The total ground state energy has its minimum at -2769.88314685 Ry as given in (Fig 3).

Table 2: The results of the total minimum energy (Ry) of CrI_3 with respect to K-points grid

K-points grid	Total Energy (Ry)
1×1×1	-2769.85820967
2×2×1	-2769.88424575
3×3×1	-2769.88302060
4×4×1	-2769.88309079
5×5×1	-2769.88313581
6×6×1	-2769.88298937
7×7×1	-2769.88314685
8×8×1	-2769.88311463
9×9×1	-2769.88311164
10×10×1	-2769.88309835

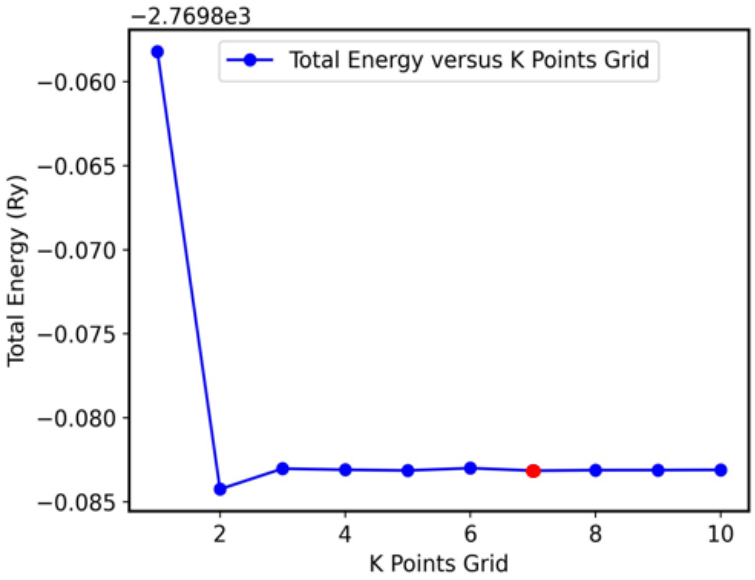

Figure 3: Graph of total minimum energy (Ry) with respect to K-point grid sampling (a.u) where 7x7x1 grid is shown to be the best converged value (red dot).

To find the equilibrium lattice constant of CrI_3, the total energy calculation was performed for a series of possible parameters. In this calculation the energy cutoff and the K-point sampling are made fixed (40 Ry, 7× 7× 1 K-point) using the energy cutoff and K-point grid criteria for energy convergence (Gabriel et al., 2020). The numerical calculation shows that the equilibrium lattice constant is 6.88 Å. This result is in a good agreement with the experimental values 6.87 Å (McGuire et al., 2015) and 6.84 Å (Li Cong; Zhang, Jihai; Chen, Shenwei; Guo, Donghui; Ji, Wei; Zhong, Dingyong, 2020) as shown in **(Fig 4).**

Table 3: The results of the total minimum energy (Ry) of CrI_3 with respect to lattice constant (a.u)

Lattice constant (Bohr)	Total energy (Ry)
11.50	-2769.33267272
12.00	-2769.65401397
12.50	-2769.82174743
13.00	-2769.87662048
13.50	-2769.87662048
14.00	-2769.82305455
14.50	-2769.74032183
15.00	-2769.64028300
15.50	-2769.53078797
16.00	-2769.41764130

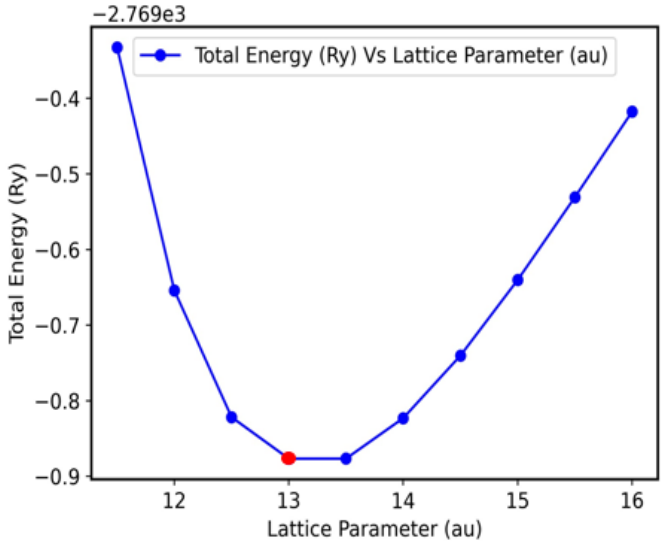

Figure 4: Equilibrium lattice constant (a.u) with respect to total energy (Ry) where 6.88 Å is found to be the best fit lattice constant (Red dot).

Structural and Magnetic Properties of Monolayer Cri_3

Monolayer CrI_3 exhibits a honeycomb crystal structure where chromium (Cr) atoms are octahedrally coordinated by iodine (I) atoms (Pokhrel, 2024). The lattice parameters of monolayer CrI_3 have been measured experimentally and predicted using DFT as indicated in Table 4. This study indicates that, the lattice constants 6.880 Å from DFT and 7.004 Å visualized using VESTA are in good agreement with experimental measurements and DFT estimations showing a remarkable consistency.

Table 4: Comparison of structural properties of CrI_3. Lattice parameter a (Å), Bond length d_{Cr_I}(Å) and bond angle $\theta_{I\text{-}Cr\text{-}I}$

Reference	Method	a (Å)	$d_{Cr\text{-}I}$ (Å)	θ (deg)
This work	PBE-spn-kpjaw	6.880		
This work	VESTA	7.004	2.737	90.627
Lado Joaquin, 2017 (Lado Joaquín, 2017)	GGA+U	6.686		
Haddadi et al., 2024 (Haddadi et al., n.d.)	PBEsol	6.817	2.692	
	PBEsol+U	6.978	2.774	
	PBEsol+U+V	6.971	2.767	
	PBEsol+$U_{\uparrow}$+$U_{\downarrow}$	6.826	2.699	
Staros et al., 2022 (Staros et al., 2022)	LS-DMC	6.870	2.723	90.400
	LDA + U	6.695		
Fayazi et al., 2022 (Fayazi et al., 2022)	GGA+U	6.930		
Qian et al., 2015 (Zhang Qian; Zhu, Peng; Lam, Chi Hang, 2015)	PBE(HSE06)	7.008		

Cong et al., 2020 (Li Cong; Zhang, Jihai; Chen, Shenwei; Guo, Donghui; Ji, Wei; Zhong, Dingyong, 2020)	Experiment	6.840	
McGuire et al., 2015 (McGuire et al., 2015)	Experiment	6.870	2.727

CrI_3 is recognized as a ferromagnetic semiconductor with a Curie temperature around 45 K (Wu et al., 2019). The ground state of monolayer CrI_3 is primarily ferromagnetic under compression but transitions to an antiferromagnetic state when subjected to tensile strain (Yang et al., 2018). This transition occurs at approximately 1.8% in-plane strain, highlighting the tunability of its magnetic properties through mechanical manipulation (Rahman, 2023). This study computed and compare the ferromagnetic moment of CrI_3 with other studies as reported in Table 5.

Table 5: The average magnetic properties of CrI_3 in this work and previous theoretical and experimental results. μ_B is the average magnetic moment of CrI_3.

Reference	Method	μ_B
This work (monolayer)	PBE-spn-kpjaw	3.56
Lado et al.,, (2017)	GGA+U	3.00
Haddadi et al., (2024)	PBEsol	3.18
	PBEsol+U	3.97
	PBEsol+U+V	3.89
	PBEsol+$U_\uparrow$+$U_\downarrow$	3.21
Staros et al., (2022)	LS-DMC	3.61
	LDA + U	3.50
Xiaolin et al., (2018)	GGA +U	3.32
Qian et al., (2015)	PBE(HSE06)	3.10
Li et al., (2024)	GGA+U	3.22
Fayazi et al., (2022)	GGA+U	3.44
Cong et al., (2020)	Experiment	3.28

The structural properties and magnetization of monolayer CrI_3 are reported in Tables 4 and 5 above. For the equilibrium lattice constant (a) (converged value) and Cr-I bond length (d_{Cr-I}) visualized using VESTA. The results exhibit closer agreement with experiments. The 6.88 Å equilibrium lattice constant is just 0.1% and 0.6% off from the experiments (Li et al., 2020) and (McGuire et al., 2015). Also, our visualized Cr-Cr lattice constant of 7.0038 Å using VESTA reveals excellent agreement with the DFT result reported by Zhang Qian using PBE (HSE06) which is just 0.06% (Zhang et al., 2015) as in the Figure 5. The Cr-I nearest distance 2.73710 Å is in agreement to both previous DFT and experimental values as illustrated in the table 4. and figure 5. Although, bond angles have not been measured experimentally in the monolayer and are scantily reported in DFT studies, our studies visualized the value for the I-Cr-I to be 90.627° which is almost the same with 90.400° by Staros et at., (2020) as shown in Table 4. Above with just 0.2% difference. All our line research falls less 3% in line with the previous derived-DFT estimation and experimental finding.

For the magnetic moment reported in Table 5, some previous DFT estimated the magnetic moment to be 3 μB across the entire CrI_3 unit, this lead to many researchers to conclude that all of the unit cell's magnetism could be attributed to that from the Cr site (Staros et al., 2022) charge that one would intuitively surmise based upon Chromium's typical oxidation state, but our DFT computed the magnetic moment on each Cr to be 3.56 μB. Interestingly, this indicates that each Cr possesses a magnetic moment sufficiently larger than that of the +3 μB. These discrepancies may arise due to the different method adopted. Our computed magnetic moment is relatively higher than that reported experimentally by Cong et al., (2020) but

almost the same with that reported by Staros et al., (2022). The magnetic moment calculations by Haddadi et al., (2024) using different methods produced a range of results, including values below, above, and close to the experimental value, as well as the value reported in this work, as detailed in Table 5.

The Structure of Three Magnetic Faces of Monolayer CrI_3 (AFM, FM and NM)

Monolayer CrI_3 has a hexagonal lattice structure, consisting of Chromium (Cr) atoms sandwiched between two layers of Iodine (I) atoms (Mak et al., 2019). The Cr atoms form a honeycomb lattice, with each Cr atom bonded to six neighboring I atoms. Monolayer CrI_3 exhibits long-range ferromagnetic ordering, with a Curie temperature (TC) around 45 K (Xue et al., 2019). The magnetic moments are oriented perpendicular to the plane, resulting in an out-of-plane magnetization. The magnetic properties change significantly with the number of layers. Bilayer and thicker CrI_3 exhibit antiferromagnetic behavior (layer-dependent magnetism) (Faculty, 2021).

The anti-ferromagnetic structure of monolayer CrI_3 arises from the alignment of Chromium's magnetic moments. Each Cr atom has a magnetic moment due to its unpaired electrons (Shabbir et al., 2018). The magnetic moments are aligned anti-ferromagnetically, meaning they point in opposite direction. The magnetic moment of 3.51 μB was calculated using DFT. Figure 6 displayed the crystal structure of AFM CrI_3.

The ferromagnetic structure of monolayer CrI_3 arises from the alignment of Chromium's magnetic moments. Each Cr atom has a magnetic moment due to its unpaired electrons. The magnetic moments are aligned ferromagnetically, meaning they point in the same direction (Shabbir et al., 2018). Figure 7 displayed the crystal structure of FM CrI_3.

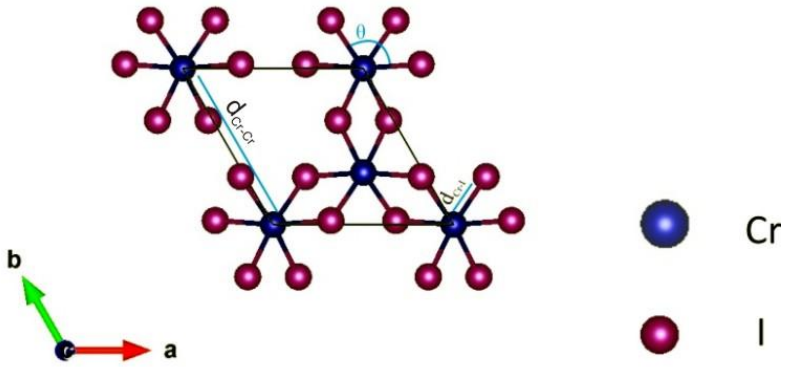

Figure 5: Crystal structure of NM of monolayer CrI_3 where bond lengths and bond angle are shown.

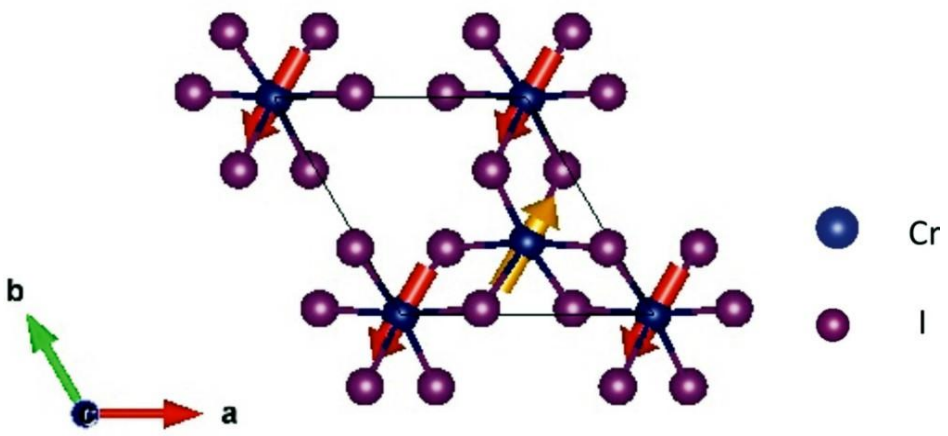

Figure 6: Structural View of AFM Monolayer CrI_3 where the magnetic moment of three Cr atoms are aligned in outward direction while one Cr atom is aligned in inward direction opposite to the three atoms.

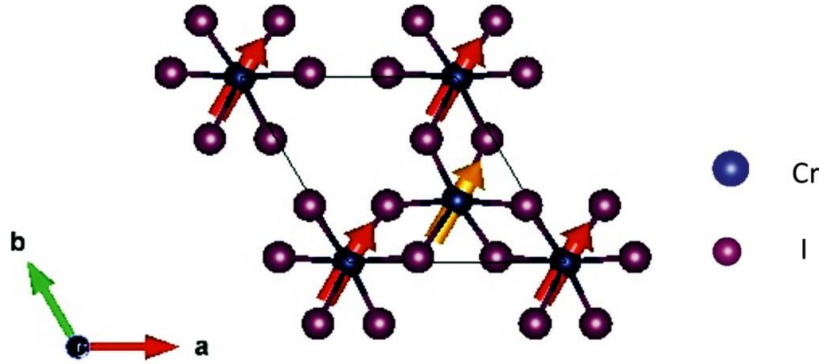

Figure 7: Structural View of FM Monolayer CrI_3 where all the atoms are aligned in the same direction.

CONCLUSION

We have determined the optimized lattice constant, K-point grid, and energy cutoff for monolayer CrI_3. Our density functional theory (DFT) calculations yield structural and magnetic properties that are in excellent agreement with previous DFT studies and experimental results, with little deviations. Notably, this work pioneers the application of the PBE-spn-kjpaw pseudopotential approach to monolayer CrI_3. The displayed structures reveal a clear magnetic alignment. For anti-ferromagnetism the moments are aligned in different directions while for ferromagnetism the moments are aligned in same direction.

It is recommended that; same studies can be extended to other Chromium Halides like $CrBr_3$ and $CrCl_3$. This will pave a way for exploring the structural and magnetic properties of other 2D-materials which can be used for spintronics, photoelectronics and thermoelectronics applications.

ACKNOWLEDGEMENT

We extend our heartfelt gratitude to the Tertiary Education Trust Fund (TETFund) Yobe State University for their generous sponsorship. We also appreciate the invaluable support of Senator Ahmad Ibrahim Lawan GCON (Sardaunan Bade), former President of the 9th Assembly, Federal Republic of Nigeria.

REFERENCES

Aslam, S., Bakhsh, S., Yusof, Y., Rahman, M. Y. A., Ibrahim, A. R., & Samsuri, S. A. M. (2023). Structural and optical properties of vacancy-ordered double halide perovskites, Cs2TiI6 films. *Materials Science and Engineering: B*, *296*(June). https://doi.org/10.1016/j.mseb.2023.116645

Blöchl, P. E. (1994). Projector augmented-wave method. *Physical Review B*, *50*(24), 17953–17979. https://doi.org/10.1103/PhysRevB.50.17953

Chen, Y., Zhang, L., Wang, H., & Weinan, W. (2020). Ground State Energy Functional with Hartree-Fock Efficiency and Chemical Accuracy. *Journal of Physical Chemistry A*, *124*(35), 7155–7165. https://doi.org/10.1021/acs.jpca.0c03886

Daga, L. E., Civalleri, B., & Maschio, L. (2020). Gaussian Basis Sets for Crystalline Solids: All-Purpose Basis Set Libraries vs System-Specific Optimizations. *Journal of Chemical Theory and Computation*, *16*(4), 2192–2201. https://doi.org/10.1021/acs.jctc.9b01004

Faculty, A. (2021). *Magnetic properties of CrI 3 monolayers , bilayers and twisted bilayers*.

Fayazi, Y., Jacobsson, L., & Gustafsson, E. F. (2022). *First principles studies of 2D magnets*. http://www.teknat.uu.se/student

Gabriel, J. J., Congo, F. Y. C., Sinnott, A., Mathew, K., Allison, T. C., Tavazza, F., & Hennig, R. G. (2020). *Uncertainty Quantification for Materials Properties in Density Functional Theory with k-Point Density*. 1–12. http://arxiv.org/abs/2001.01851

Giannozzi, P., Baroni, S., Bonini, N., Calandra, M., Car, R., Cavazzoni, C., Ceresoli, D., Chiarotti, G. L., Cococcioni, M., Dabo, I., Dal Corso, A., De Gironcoli, S., Fabris, S., Fratesi, G., Gebauer, R., Gerstmann, U., Gougoussis, C., Kokalj, A., Lazzeri, M., … Wentzcovitch, R. M. (2009). QUANTUM ESPRESSO: A modular and open-source software project for quantum simulations of materials. *Journal of Physics Condensed Matter*, *21*(39). https://doi.org/10.1088/0953-8984/21/39/395502

Gibertini, M., Koperski, M., Morpurgo, A. F., & Novoselov, K. S. (2019). Magnetic 2D materials and heterostructures. *Nature Nanotechnology*, *14*(5), 408–419. https://doi.org/10.1038/s41565-019-0438-6

Haddadi, F., Linscott, E., Timrov, I., Marzari, N., & Gibertini, M. (n.d.). *On-site and inter-site Hubbard corrections in magnetic monolayers: The case of FePS 3 and CrI 3*. 1–18.

Halperin, B. I. (2019). On the Hohenberg–Mermin–Wagner Theorem and Its Limitations. *Journal of Statistical Physics*, *175*(3–4), 521–529. https://doi.org/10.1007/s10955-018-2202-y

Hamann, D. R. (2013). Optimized norm-conserving Vanderbilt pseudopotentials. *Physical Review B - Condensed Matter and Materials Physics*, *88*(8), 1–21. https://doi.org/10.1103/PhysRevB.88.085117

Huang, B., Clark, G., Navarro-Moratalla, E., Klein, D. R., Cheng, R., Seyler, K. L., Zhong, Di., Schmidgall, E., McGuire, M. A., Cobden, D. H., Yao, W., Xiao, D., Jarillo-Herrero, P., & Xu, X. (2017). Layer-dependent ferromagnetism in a van der Waals crystal down to the monolayer limit. *Nature*, *546*(7657), 270–273. https://doi.org/10.1038/nature22391

Huang, P., Zhang, P., Xu, S., Wang, H., Zhang, X., & Zhang, H. (2020). Recent advances in two-dimensional ferromagnetism: Materials synthesis, physical properties and device applications. *Nanoscale*, *12*(4), 2309–2327. https://doi.org/10.1039/c9nr08890c

Irfan, B. (2021). Spintronics: Overview on Spin Based Electronics and Its Potential Applications. *International Journal of Materials Science and Applications*, *10*(5), 94. https://doi.org/10.11648/j.ijmsa.20211005.11

Kaur, L., & Mandal, D. (2024). A density functional theory analysis of the C-H activation reactivity of iron(iv)-oxo complexes with an 'O' substituted tetramethylcyclam macrocycle. *Dalton Transactions*, *53*(17), 7527–7535. https://doi.org/10.1039/d4dt00063c

Lado Joaquín, J. L. . F.-R. (2017). On the origin of magnetic anisotropy in two dimensional

CrI3. *2D Materials*, *4*(3), 035002-NA. https://doi.org/10.1088/2053-1583/aa75ed

Li Cong; Zhang, Jihai; Chen, Shenwei; Guo, Donghui; Ji, Wei; Zhong, Dingyong, P. W. (2020). Single-layer CrI3 grown by molecular beam epitaxy. *Science Bulletin*, *65*(13), 1064–1071. https://doi.org/10.1016/j.scib.2020.03.031

Li, H., Ruan, S., & Zeng, Y. J. (2019). Intrinsic Van Der Waals Magnetic Materials from Bulk to the 2D Limit: New Frontiers of Spintronics. *Advanced Materials*, *31*(27), 1–34. https://doi.org/10.1002/adma.201900065

Mak, K. F., Shan, J., & Ralph, D. C. (2019). Probing and controlling magnetic states in 2D layered magnetic materials. *Nature Reviews Physics*, *1*(11), 646–661. https://doi.org/10.1038/s42254-019-0110-y

Mañes, J. L. (2012). Existence of bulk chiral fermions and crystal symmetry. *Physical Review B - Condensed Matter and Materials Physics*, *85*(15). https://doi.org/10.1103/PhysRevB.85.155118

McGuire, M. A., Dixit, H., Cooper, V. R., & Sales, B. C. (2015). Coupling of crystal structure and magnetism in the layered, ferromagnetic insulator cri3. *Chemistry of Materials*, *27*(2), 612–620. https://doi.org/10.1021/cm504242t

Mermin, N. D., & Wagner, H. (1966). Absence of ferromagnetism or antiferromagnetism in one- or two-dimensional isotropic Heisenberg models. *Physical Review Letters*, *17*(22), 1133–1136. https://doi.org/10.1103/PhysRevLett.17.1133

Momma, K., & Izumi, F. (2011). *VESTA 3 for three-dimensional visualization of crystal , volumetric and morphology data*. 1272–1276. https://doi.org/10.1107/S0021889811038970

Novoselov Artem; Carvalho, Alexandra; Neto, A. H. Castro, K. S. . M. (2016). 2D materials and van der Waals heterostructures. *Science (New York, N.Y.)*, *353*(6298), 461. https://doi.org/10.1126/science.aac9439

Olsen, T. (2019). Theory and simulations of critical temperatures in CrI3 and other 2D materials: Easy-axis magnetic order and easy-plane Kosterlitz-Thouless transitions. *MRS Communications*, *9*(4), 1142–1150. https://doi.org/10.1557/mrc.2019.117

Pocs, C. A., Leahy, I. A., Zheng, H., Cao, G., Choi, E. S., Do, S. H., Choi, K. Y., Normand, B., & Lee, M. (2020). Giant thermal magnetoconductivity in CrCl3 and a general model for spin-phonon scattering. *Physical Review Research*, *2*(1), 1–13. https://doi.org/10.1103/PhysRevResearch.2.013059

Pokhrel, S. (2024). No TitleΕΛΕΝΗ. *Αγαη*, *15*(1), 37–48.

Rahman, S. (2023). *N - a t n 2d m t h*. *March*.

Retegan, M., Jafri, S. F., Curti, L., Lisnard, L., Otero, E., Rivière, E., Haverkort, M. W., Bleuzen, A., Sainctavit, P., & Arrio, M. A. (2023). Orbital Magnetic Moment and Single-Ion Magnetic Anisotropy of the S = 1/2 K3[Fe(CN)6] Compound: A Case Where the Orbital Magnetic Moment Dominates the Spin Magnetic Moment. *Inorganic Chemistry*, *62*(46), 18864–18877. https://doi.org/10.1021/acs.inorgchem.3c02158

Reyes-Martinez, M. A., Tan, P., Kakekhani, A., Banerjee, S., Zhumekenov, A. A., Peng, W., Bakr, O. M., Rappe, A. M., & Loo, Y. L. (2020). Unraveling the Elastic Properties of (Quasi)Two-Dimensional Hybrid Perovskites: A Joint Experimental and Theoretical Study. *ACS Applied Materials and Interfaces*, *12*(15), 17881–17892. https://doi.org/10.1021/acsami.0c02327

Shabbir, B., Nadeem, M., Dai, Z., Fuhrer, M. S., Xue, Q. K., Wang, X., & Bao, Q. (2018). Long range intrinsic ferromagnetism in two dimensional materials and dissipationless future technologies. *Applied Physics Reviews*, *5*(4), 1–36. https://doi.org/10.1063/1.5040694

Singh, B., Kumar, D., Manna, K., Bera, A. K., Cansever, G. A., Maljuk, A., Wurmehl, S., Büchner, B., & Kumar, P. (2019). Correlated paramagnetism and interplay of magnetic and phononic degrees of freedom in 3d-5d coupled La2CuIrO6. *Journal of Physics Condensed Matter*, *31*(48), 1–24. https://doi.org/10.1088/1361-648X/ab3c14

Song, N. H., Wang, Y. S., Zhang, L. Y., Yang, Y. Y., & Jia, Y. (2018). Density functional theory study of tunable electronic and magnetic properties of monolayer BeO with intrinsic vacancy and transition metal substitutional doping. *Journal of Magnetism and Magnetic Materials*, *468*, 252–258. https://doi.org/10.1016/j.jmmm.2018.08.019

Staros, D., Hu, G., Tiihonen, J., Nanguneri, R., Krogel, J., Bennett, M. C., Heinonen, O., Ganesh, P., & Rubenstein, B. (2022). A combined first principles study of the structural, magnetic, and phonon properties of monolayer CrI3. *Journal of Chemical Physics*, *156*(1). https://doi.org/10.1063/5.0074848

Study, A. C., Wang, B., Yan, X., Cui, X., & Cai, Y. (2022). *First-principles Study of Phonon Lifetime and Low Lattice Thermal First-Principles Study of the Phonon Lifetime and Low Lattice Thermal Conductivity of Monolayer γ - GeSe : A Comparative Study*. *October*. https://doi.org/10.1021/acsanm.2c03476

Tomar, S., Rastogi, P., Bhadoria, B. S., Bhowmick, S., Agarwal, A., Chauhan, Y. S., & Structure, A. C. (n.d.). *Thermoelectric Properties of CrI 3 Monolayer*. *1*(d), 1–4.

Tomarchio, L., Mosesso, L., Macis, S., Nguyen, L. T., Grilli, A., Romani, M., Cestelli Guidi, M., Cava, R. J., & Lupi, S. (2023). Phonon Anharmonicity and Spin–Phonon Coupling in CrI3. *Materials*, *16*(14), 1–10. https://doi.org/10.3390/ma16144909

Wang, D., & Sanyal, B. (2021). *Systematic Study of Monolayer to Trilayer CrI 3 : Stacking Sequence Dependence of Electronic Structure and Magnetism*. https://doi.org/10.1021/acs.jpcc.1c04311

Wang, Y., Wisesa, P., Balasubramanian, A., Dwaraknath, S., & Mueller, T. (2021). Rapid generation of optimal generalized Monkhorst-Pack grids. In *Computational Materials Science* (Vol. 187). https://doi.org/10.1016/j.commatsci.2020.110100

Webster, L., & Yan, J. A. (2018). Strain-tunable magnetic anisotropy in monolayer CrCl3, CrBr3, and CrI3. *Physical Review B*, *98*(14). https://doi.org/10.1103/PhysRevB.98.144411

Wu Jin; Yuan, Shengjun, Z. Y. (2019). Strain-tunable magnetic and electronic properties of monolayer CrI3. *Physical Chemistry Chemical Physics : PCCP*, *21*(15), 7750–7755. https://doi.org/10.1039/c8cp07067a

Xue, F., Hou, Y., Wang, Z., & Wu, R. (2019). Two-dimensional ferromagnetic van der Waals CrC l3 monolayer with enhanced anisotropy and Curie temperature. *Physical Review B*, *100*(22). https://doi.org/10.1103/PhysRevB.100.224429

Yang Xiaolin; Yang, Hongxin; Han, Xiufeng; Yan, Yu, B. Z. (2018). Nonmetallic Atoms Induced Magnetic Anisotropy in Monolayer Chromium Trihalides. *The Journal of Physical Chemistry C*, *123*(1), 691–697. https://doi.org/10.1021/acs.jpcc.8b09939

Yang, Y., Li, P., Wang, W., & Zhang, X. (2021). First-principles study on the electronic properties and enhanced ferromagnetism of alkali metals adsorbed monolayer CrI3. *Vacuum*, *194*(August), 110561. https://doi.org/10.1016/j.vacuum.2021.110561

Zhang Qian; Zhu, Peng; Lam, Chi Hang, W.-B. Q. (2015). Robust Intrinsic Ferromagnetism and Half Semiconductivity in Stable Two-Dimensional Single-Layer Chromium Trihalides. *Journal of Materials Chemistry C*, *3*(48), 12457–12468. https://doi.org/10.1039/c5tc02840j